Available online at www.sciencedirect.com
ScienceDirect
Proceedings of the Combustion Institute 33 (2011) 3233–3240
Proceedings of the Combustion Institute
www.elsevier.com/locate/proci

Combustion dynamics for energetically enhanced flames using direct microwave energy coupling

Xing Rao [a], Kadek Hemawan [b], Indrek Wichman [a], Campbell Carter [c], Timothy Grotjohn [b], Jes Asmussen [b], Tonghun Lee [a,*]

[a] Department of Mechanical Engineering, Michigan State University, East Lansing, MI 48824, USA
[b] Department of Electrical & Computer Engineering, Michigan State University, East Lansing, MI 48824, USA
[c] Air Force Research Laboratory, Wright-Patterson AFB, OH 45433, USA

Available online 6 August 2010

Abstract

An atmospheric high-Q re-entrant cavity applicator is used to couple microwave (2.45 GHz) electromagnetic energy directly into the reaction zone of a premixed laminar methane–oxygen flame for flame enhancement. As microwave energy increases, a transition from electric field enhancement to microwave plasma discharge is observed. At low microwave powers (1–5 W), the flame is influenced by an electromagnetic field only. When power is increased, ionization and eventually breakdown of gas molecules result in a plasma plume with significant increase in the flammability limit. 2-D laser induced fluorescence imaging of hydroxyl radicals (OH) and carbon monoxide (CO) are conducted in the reaction zone over this transition, as well as spectrally resolved flame emission measurements to monitor excited state species and derive rotational temperatures using OH chemiluminescence for a range of equivalence ratios ($\phi = 0.9$–1.1) and total flow rates. In the electromagnetic field only phase (1–5 W), flame stability, excited state species, and temperature slightly increased with power while no significant change in OH number density was detected. With the onset of a plasma plume, a significant rise in both excited state species, CO and OH number density was observed. The importance of in-situ fuel reforming in plasma coupled flames is shown through the concentration of CO, which increases ~18% with 30 W microwave power.
© 2010 The Combustion Institute. Published by Elsevier Inc. All rights reserved.

Keywords: Plasma enhanced combustion; Microwave; Hydroxyl; Carbon monoxide; Laser induced fluorescence

1. Introduction

The use of electromagnetic energy and non-equilibrium plasma in particular for enhancing ignition and combustion stability are receiving increased attention due to their potential for enabling highly efficient thermal energy conversion, extension of the flammability limit, reliable ignition in harsh operating conditions, integration of alternative fuels with variations in burning characteristics [1,2], and for development of next generation hypersonic propulsion systems [3,4]. From a practical perspective, a light-weight power supply and discharge unit can be easily integrated into a combustion system, and the non-equilibrium aspect of the discharge can efficiently target energy transfer to boost the combustion chemistry.

* Corresponding author. Address: 2555 Engineering Building, Michigan State University, East Lansing, MI 48840 USA. Fax: +1 517 432 3341.
E-mail address: Tonghun@msu.edu (T. Lee).

1540-7489/$ - see front matter © 2010 The Combustion Institute. Published by Elsevier Inc. All rights reserved.
doi:10.1016/j.proci.2010.06.024

The exact mechanism for flame enhancement by a plasma is still being actively studied, but a number of studies have provided a glimpse into various aspects of this process [5–11]. It appears that the electromagnetic energy alters the reaction chemistry by: (1) decomposition of the fuel from larger to smaller hydrocarbons and creation of radicals via collision with electrons; (2) radiation-induced electron excitation; (3) increased flame temperature by ohmic heating; (4) increase in excited state species, ions and electrons; and (5) in-situ fuel reformation. The prospect of gaining insight into the synergistic integration of electrodynamics and combustion chemistry is a formidable challenge and requires further work. An extensive review can be found in [1].

In this study we investigate the direct coupling of electromagnetic energy into the reaction zone of an existing premixed flame for energetic enhancement of the combustion chemistry, and to extend operation limits during transient or harsh loading conditions. The plasma generation process can be achieved with minimal power, as a high electric field is directly coupled to the electrons naturally present in a hydrocarbon-based flame. Our goal is to understand the changes in the chemistry and temperature during this process including the impact of in-situ fuel reforming into CO and H_2, which is proposed as a key flame stabilization mechanism [8].

2. Experimental setup

2.1. Coaxial re-entrant cavity applicator

A unique coaxial re-entrant cavity applicator was developed for coupling microwave energy directly into the reaction zone. The details regarding this torch have been previously described [12] and only a brief summary will be given here. In Fig. 1 we show the coaxial re-entrant cavity applicator: (a) displays a photograph of the system along with an inset picture of a methane/oxygen flame; (b) displays the corresponding schematic. The applicator is a brass re-entrant cavity excited with TEM electromagnetic fields in the quarter wavelength resonance mode in the TEM mode [13] and includes the following components: (1) brass gas tube burner; (2) adjustable endplate; and (3) mono-pole antenna loop. Positions of all three components are set using a micrometer-actuated unislide translator with an accuracy of 0.01 mm. This redesign of our previous system [12] has a modified tip around the main chamber that enhances focus of the microwave energy into the flame reaction zone.

2.45 GHz microwave energy is transmitted via a coaxial cable and emitted with a mono-pole antenna (Fig. 1b). When the relative location of the torch, antenna, and baseplate are adjusted

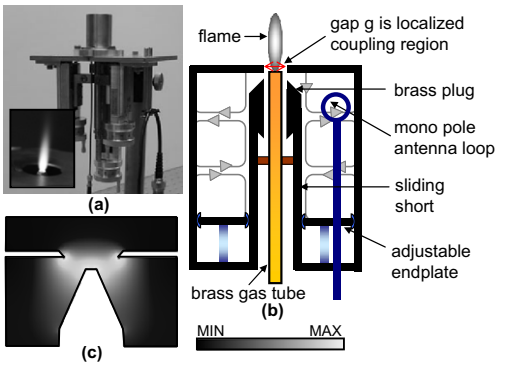

Fig. 1. (a) Picture of coaxial re-entrant cavity applicator with picture of methane/oxygen flame shown in the inset; (b) figure of the structure of the applicator; (c) numerical simulation of electric field using COMSOL MultiPhysics.

using the Unislide translators, an optimized resonant mode can be found wherein most of the energy is focused into the region between the edge of the outer cavity and the end of the combustion torch. Further details regarding simulations to optimize the orientation of the electrical field will be presented in the next section. Among several nearby TEM modes, we select one that allows the center torch to be exposed outside the main chamber, so that the flame is clearly visible and can accommodate laser and optical diagnostics. The chamber itself is 35 mm in diameter and is generally optimized to a height of around 3 cm.

The overall size and geometry of the re-entrant cavity applicator, chosen/designed to enable coupling of the microwave energy into the reaction zone of the flame, was based on numerical simulation of the electric field propagation. Figure 1(c) show a numerical solution of Maxwell's equations using the "Rf Electromagnetic Solver" module of the program COMSOL MultiPhysics 3.4 with *2.45* GHz microwave excitation. This provided a relative *2-D* electric field distribution within the coaxial cavity structure. For our simulations, the medium inside the cavity is air, and all boundaries are set to be perfect electrical conductors. The focus of the electromagnetic energy into the tip of the torch is enhanced as the radicals and the weak concentration of electrons in the flame amplify the coupling process. Different cavity geometries were tested and a sharp knife-edge was selected. The E field simulation shows intense electric field at the end of the torch (reaction zone) and the sharp edge of the cavity. In practice, this type of mode can be used to focus the microwave energy when a flame sits on top of the burner exit. The tip of the burner can be raised to be almost flush with the cavity surface so that the flame is fully exposed for study using optical and laser diagnostics.

2.2. Diagnostics methods

A schematic diagram of the laser diagnostics and microwave power setup is shown in Fig. 2. UV laser near 283 nm was used for planar laser induced fluorescence (PLIF) of OH using the $Q_1(8)$ transition from $A^2\Sigma^+$–$X^2\Pi$ (1, 0) [14]. The measurements were conducted using a dye laser (Lumonics Hyperdye HD-300). R590 dye from Exciton was used for generating pulses at 566 nm, which is frequency doubled through an Inrad Autotracker (ATIII) to a final output frequency of 283 nm (linewidth $\sim$0.1 cm^{-1}). The 283-nm beam is isolated from the 566-nm beam within an Inrad Prism Harmonic Separator (PHS). The laser was expanded into a sheet and the fluorescence signal was collected at 90° using an intensified CCD camera with a WG305 filter. The number density was derived by calibrating the signal to that of a Hencken Burner using a methane–air mixture. Here, it was assumed that the fluorescence was in the linear regime; accordingly the OH number density was further corrected for differences in the rates for electronic quenching between the methane–oxygen flames and Hencken calibration flame using estimates of quenching rates from the OH A–X transition [15]. It should be noted that the reported cross sections describe quenching from $A(v' = 0)$, whereas fluorescence is derived from both the A–X ($v' = 1, v'' = 1$) and (0, 0) bands after excitation to $A(v' = 1)$.

CO in the reaction was measured using two-photon PLIF, pumping the $B^1\Sigma^+$–$X^1\Sigma^+$ (0, 0) transition at 230.10 nm [16]. The 532 nm beam from a Newport Nd:YAG was used to pump a Sirah Precisionscan LG-2400 dye laser operating with Exciton DCM dye. The 653-nm output of dye laser was sum-frequency-mixed with the third harmonic beam (355 nm) from the injection seeded Nd:YAG laser to produce 230 nm radiation (linewidth $\sim$0.1 cm^{-1}) needed for two-photon laser induced fluorescence. The pulse energy is recorded digitally using an energy monitor from LaVision.

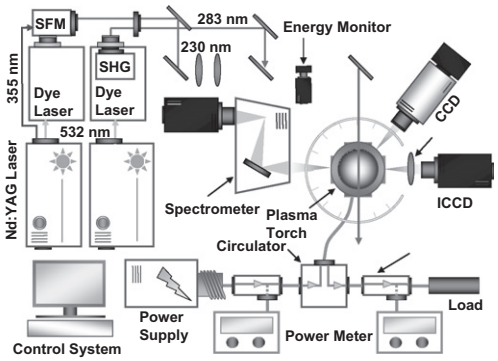

Fig. 2. Experimental setup with bottom part shows microwave energy generation, coupling and monitor system.

The fluorescence signal was imaged with an interference filter centered at 486 nm with a bandwidth of 10 nm. The number density is calibrated from a Chemkin simulation (mole fraction for 0 W microwave power) using GRI-mech 3.0 [17] with 1-D flame modeling with methane and oxygen. Equilibrium values past the reaction zone are used as a first order approximation of the Bunsen Flame geometry of our flame. Here, it was assumed that the rate for photo-ionization, from a third photon at 230 nm, dominated the rate for electronic quenching and that no quenching correction was therefore needed.

A McPherson 216.5 1-m spectrometer (entrance slit of 20 μm) was used for flame emission measurements and rotational OH thermometry. The emission was focused using a spherical lens ($f = 50$ mm) through a pin-hole filter to isolate the reaction zone. A wide-range scan was conducted over a range of 250–550 nm at an increment of 0.5 nm to monitor the qualitative change in the population of excited state species.

In the current study, a methane/oxygen flame is used to simplify the reaction chemistry, by excluding nitrogen reactions. The microwave generation system consists of a power supply (Raytheon Model PGM10X1) and modules to measure incident and reflected power as shown in the lower portion of Fig. 2. This allows us to compute the coupling efficiency from the ratio of the incident and reflected powers. The optimization of the efficiency generally involves a slight tuning of the cavity geometry using the three adjustments involving the torch, cavity base plate, and the loop antenna.

3. Results and discussion

3.1. Impact on flame structure and radical concentration

Photographs, 2-D OH PLIF and CO PLIF images of the flame are shown in Fig. 3 as a function of increasing microwave power. At this condition, the fuel combustion power is 22 W using the lower heating value of methane. The plasma plume is established in a uniform glow mode and micro-arc transition for certain conditions outside our operating conditions. Overall, the flame luminosity and volume is increased as more microwave power is coupled into the flame region. At low powers the flame length is about 2 mm and a typical light blue hue is observed from the CH^* emission. As the power is raised to about 6 W, the microwave energy generates a distinctly different plasma plume with a purple emission that can be up to 10 mm in length (top row in Fig. 3). From the OH images (middle row), it can be seen that the location of the reaction zone does not change dramatically, and only a significant rise of OH in the post-combustion gas region is evident. It is expected that emission from

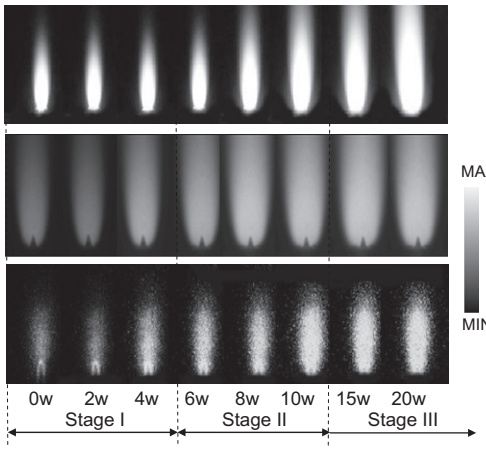

Fig. 3. Emission (top), OH PLIF (middle) and CO PLIF (bottom) intensity images of CH_4/O_2 flame vs. microwave power with three stages noted (100 SCCM total flowrate at $\phi = 1.1$).

a dramatic increased ionization and excited state species dominates the normal visible emission spectra at this point. The progression of the plasma discharge as a function of microwave power can be divided into three distinct stages, which we will refer to throughout the rest of this publication. Note that the microwave power listed here generates a volumetric discharge around the flame and only a fraction of the energy is actually coupled into the reaction zone.

- *Stage 1:* "Electric Field Enhanced Stage": The flame is influenced by only a weak electric field and the input microwave power is below 6 W. No visual change can be seen in either the photographs or the OH PLIF images as the power is increased.
- *Stage 2:* "Transition Stage": Between 6 and 10 W, the plasma discharge and flame exist at the same time, and the discharge volume is dramatically increased. Near the end of this range, the system can sustain a plasma plume even if the combustion gas is discontinued. The plume can re-ignite a flame if combustible mixtures are reintroduced. Intensity of both OH and CO is increased. The reduced electric field concentration is above the critical threshold required for breakdown and is in the range of 10^{7-8}V/m. The distribution of the electric field was shown in Fig. 1.
- *Stage 3:* "Full Plasma Stage": If microwave energy input exceeds 10 W, the system enters a stage where the plasma plume dominates, and the discharge emits a pink hue. As the power is further raised, the volumetric discharge of the plasma is increased and the emission transitions to a more pink–purple hue. The discharge has a uniform glow when viewed using an intensified CCD camera with gate times down to several nanoseconds.

Without a flame present, the microwave energy cannot by itself couple into the air and generate a plasma plume in the power ranges discussed here.

In all three stages microwave energy is coupled into the flame via energy transfer from the input microwave energy source into the electron gas. This energy transfer then raises the electron gas temperature – creating a non-equilibrium chemistry condition in all three stages. The electron gas transfers its energy via electron – heavy molecule elastic and inelastic collisions processes into the heavier molecular gases. The main differences for these three stages are that electrons in Stage 1 are mostly come from flame only whereas in Stage 2 and 3, the electron are believed to increase by 1–2 order of magnitude (from $\sim 10^{10}$ cm^{-3} to $\sim 10^{11-12}$ cm^{-3}).

To quantify the change in the OH radical over the entire range of microwave powers in more detail, the number density of OH in the reaction zone of the flame is shown in Fig. 4. The region of data extraction in the PLIF image is shown in the inset and is mainly from the reaction zone of the flame. OH number density is plotted as a function of microwave power (0–30 W) for different total flow rates and equivalence ratios. The data is extracted from OH 2-D PLIF images which have been averaged over 200 single shots and calibrated for variations in laser energy. For each data set (0–30 W at same total flow rate and equivalence ratio), the same general trend over the three stages can be observed. At the same equivalence ratio ($\phi = 0.9$ or 1.1), OH number density increases with total flow rate. Also at the same total flow rate (60 or 100 SCCM), OH number density for $\phi = 0.9$ is higher than that for $\phi = 1.1$.

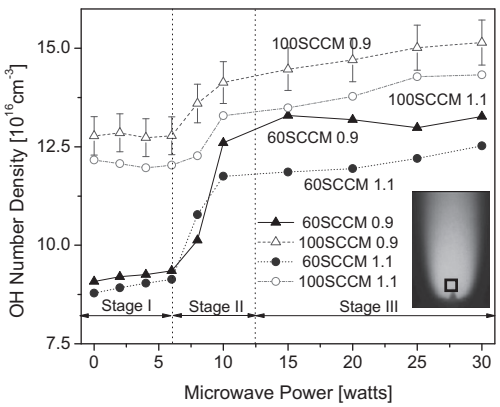

Fig. 4. OH number density in burnt gas of CH_4/O_2 flame vs. microwave powers from averaged PLIF images.

- *Stage 1:* "Electric Field Enhanced Stage": In the first stage (0–6 W), the OH does not show a noticeable increase when the measurement uncertainty is considered (~8%). There is insufficient microwave energy to generate a cascade of ionization leading to a plasma discharge. Nonetheless, both flame speed and stability is enhanced (discussed further in the next section) mainly through temperature rise from elastic collisions and in-situ reforming (section 3.4).
- *Stage 2:* "Transition Stage": In this stage (6–10 W), as the microwave field intensity increases, T_e (electron temperature) exceeds T_g (gas temperature). High T_e and high reactivity lead to inelastic collisions for excitation, dissociation and ionization to generate new species and eventually break down to generate a plasma discharge.
- *Stage 3:* "Full Plasma Stage": In the third stage (more than 10 W), the plasma volume grows larger and OH production remains relatively constant even though microwave powers are different.

It can be seen by quantifying the slope of OH increase with respect to power input, for 60 SCCM total flow rate, the slope for Stage 2 is 4 times bigger than that in Stage 1 and 20 times bigger than that in Stage 3. For 100 SCCM, the change in slope is not as dramatic although Stage 2 is still the region of maximum change rate.

It is believed that in plasma enhanced flames, free electrons are generated in the flamefront through reaction $CH + O \rightarrow HCO^+ + e^-$ [18,19]. At higher total flow rates, more heat release from combustion with relatively less heat loss to burner leads to higher temperatures, which results in more CH and subsequently more electrons. This results in more OH production for higher flowrates in Stage 2 of Fig. 3. In Stage 1, the microwave power is not high enough to generate more atomic oxygen.

The other important pathways for OH production in Stage 2 are $H_2O + e^- \rightarrow e^- + H + OH$, $H_2O + O \rightarrow OH + OH$, and $H + O_2 \rightarrow OH + O$ [20]. Atomic oxygen is believed to increase in plasma coupled combustions more than in combustion only cases [10] (increased from the order of 10^{-5} in mole fraction without plasma discharge to 10^{-4} with pulsed plasma). A Chemkin simulation using GRI-mech 3.0 [17] with a premixed burner model of flame with methane and oxygen show that, with the addition of 10^{-4} mole fraction of atomic oxygen, the OH number density increases by 40%. Similar increase was observed in our experiments for both $\phi = 0.9$ and 1.1 conditions at a total flow rate of 60 SCCM.

There are three reasons for relatively stable OH number densities in Stage 3. First, even though higher microwave power creates more electrons, the increased OH by the electron impact reactions is cancelled by more space recombination as additional active species are increased. Second, the microwave coupling efficiency is lower for higher microwave powers, due to more recombination reactions. Third, even though the power is increased, the plasma volume is also increased and the power/volume ratio remains relatively constant. From a practical perspective, this would be the stage that can be utilized for both flame stability enhancement and re-ignition.

The relative uncertainty associated with the beam energy fluctuation corrections and wavelength shift of the laser is expected to be is less than ±4%. Camera readout error was suppressed by subtracting a background image taken without the laser pulse and can be neglected. Combined with the errors from the flowmeters and shot noise, the overall relative uncertainty is expected to be less than 8%. The error in the absolute accuracy is expected to be higher (10−20% range).

3.2. Flammability limits and flame speed

The addition of plasma has been shown to increase the flammability limit [21,22]. Flammability limits (both lean and rich) for this plasma discharge system with and without microwave enhancement are shown in Fig. 5. In these measurements, the total flowrate is not held constant in determining the extended oxidation limits. In the upper portion of the figure, oxygen flow rate is fixed and methane is increased to achieve the rich flammability limit. Our goal in this section is to show how much fuel can be put into and combusted with constant oxygen flow input.

In the bottom portion of the figure, the oxygen flow rate is fixed and methane is reduced to obtain

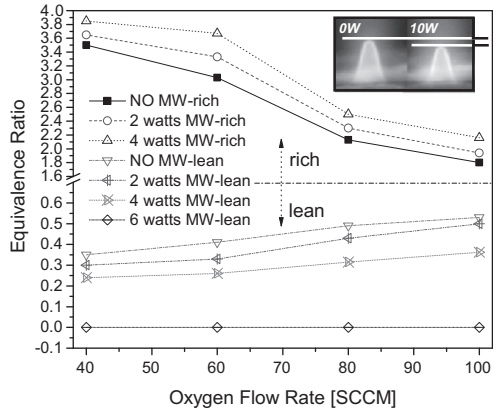

Fig. 5. Flammability limits for methane/oxygen flame (lean and rich) with flamespeed increase demonstrated by flame photographs with no microwave radiation and 10 W microwave radiation (right top).

the lean flammability limits. All the data presented in Fig. 5 are in the low-power range (0–4 W), with a flowrate spanning from 50 to 250 SCCM. Clearly we can see improvements in the flammability in this range, although the flame enhancement is only through a weak electric field. At power levels of more than 6 W, the discharge could be sustained with only oxygen or methane and without combustion. As the ground state OH number density was not shown to increase in this stage, the improvement in the flammability limit is mainly assumed to be from temperature increase, which will be discussed further in the next section.

Flamespeed enhancement was also shown in this region by observing the change in the reaction zone contour as the flame velocity was changed. An example of this is shown in the upper right inset of Fig. 5, where a photograph of the flame is shown without microwave input and with 10 W of microwave power. Here, flamespeed increase is demonstrated by a decrease in the Bunsen flame "cone" angle; this is observed in all three stages of the microwave coupling. Flamespeed enhancement using microwave fields has been observed previously in tunable microwave cavities, using free floating laminar premixed flames [23,24]. Note that in Fig. 5 the flame images look different from those in Fig. 1 due to different exposure times. In Fig. 1, longer exposure time (1/10 s) is used to integrate the emission from all the chemical species and in Fig. 5, significantly shorter exposure time (1/30 s) was used for high contrast of the flame front.

3.3. Emission measurements and temperature

In order to probe the changes in excited state species and temperature, spectrally resolved emission of the reaction zone was obtained. Figure 6 shows the emission spectra for the methane–oxygen flame with no microwave input and 10 W microwave input (top) and OH rotational temperature for different total flow rates and equivalence ratios (bottom) with top portion of Fig. 6 demonstrating a fast scan over the entire spectral range. The OH rotational temperature is calculated using a more detailed scan over the OH with a resolution of 1/30 nm and higher gain (not shown here). The general range and trend of temperatures reported here agree fairly well with a previous measurement using CH emission in a similar torch configuration [12]. As the signal is from chemically excited species, the emission intensity is a relative measure of concentration. Although, temperature corrected concentrations of excited state species are not reported here, it is clear from Fig. 6 that even without relevant temperature corrections, for 10 W of microwave power, the emission is generally higher and excited state species, such as OH and CH, have been shown previously to play an important role in the flame chemistry

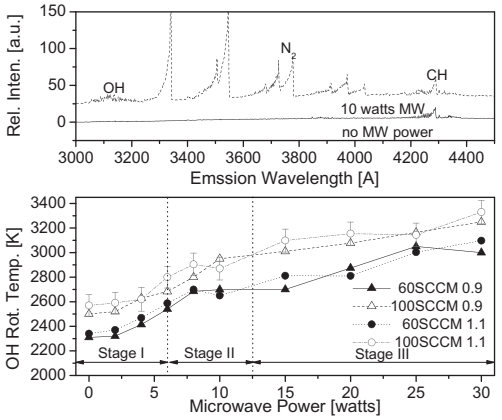

Fig. 6. Emission spectra from CH_4/O_2 flame with no microwave radiation and 10 W microwave radiation (top) and OH rotational temperature at the same conditions as in Fig. 5 (bottom).

[21,25]. Temperature measurements using CH emission were also measured for comparison and were shown to generally agree with the OH rotational temperatures (described below) and in the same range. The main choice for using OH is due to the fact that distortion from self absorption is lower for OH (smaller cross-section), and more importantly, because OH is more pervasively present past the reaction zone than CH which occupies a small portion of the flame front (note that the flame is very small).

For the reported temperatures, OH population density is determined under the assumption of Boltzmann distributions. Emission intensity I can be expressed with the following equation [26]:

$$\ln\left(\frac{I}{\lambda^4 S}\right) = -\frac{E_j}{kT} + \ln C \qquad (1)$$

where λ is the emission wavelength (nm), S is oscillator strength(Honl-London factor) (a.u.), E_i is the rotational energy of the initial level of the line (cm^{-1} or eV), k is the Boltzmann constant, C is the proportionality constant, and T is the rotational temperature. Four transitions ($R_2(14)$ (307.1145 nm), $R_2(15)$ (307.3028 nm), $R_2(4)$ (307.4369 nm), and $R_2(3)$ (307.7028 nm)) and associated constants (λ, S, E_J) are taken from [27,28] for the rotational thermometry. The overall error is expected to be about ± 100 K [27], including the fitting error. The OH^* temperatures reported here are meant to provide understanding of the change in temperature through the various stages of plasma coupling, and we acknowledge that the rotational temperatures reported here may vary from the actual translational temperature due to effects such as self absorption [29] and chemical pumping mechanisms [30] which may preferentially populate high lying rotational states in the electronically excited OH.

For microwave field enhanced combustion (Stage 1), there are different reports in the literature about the temperature change: In some cases changes of ~100 K were observed [31] whereas in other cases measurements showed no increase in rotational temperature [23]. We observed OH rotational temperature increase of around 100–150 K, which we believe is directly responsible for the observed increase of both flame speed and flammability. Overall, OH rotational temperature increases with microwave power input, which confirms the results from a previous study using CH^* [12].

The discharge power noted here is not the exact power coupled into the flame. Much of it is lost along the transmission lines and volumetric spatial microwave field distribution which is larger than the flame. We estimate that about ~40% of the power is coupled into the flame considering the electrical components of the circuit and mode of microwave propagation. Assuming constant gas composition, specific heats (products), and using rotational temperature as the overall global temperature, about half of the coupled energy is going into the temperature increase, and therefore a significant portion is coupled into the chemical energy conversion via kinetics effects. The plasma energy is calculated a fraction of the total combustion power (5–10%) and this fraction decreases with increasing power.

We acknowledge that the use of rotational temperatures over a wide range of plasma powers is subject to error and unintended influence from non-equilibrium effects. Other optical measurements such as Rayleigh scattering can be considered in the future to corroborate these findings.

3.4. In-situ fuel reforming

Figure 7 shows CO number density in the reaction zone of the CH_4/O_2 flame vs. microwave powers for total flow rate of 60 and 100 SCCM and for $\phi = 0.9$ and 1.1 from the two-photon absorption LIF (TALIF) images. The region of interest (displayed in Fig. 7) is in and around the reaction zone of the tip of the flame where CO is highest in concentration.

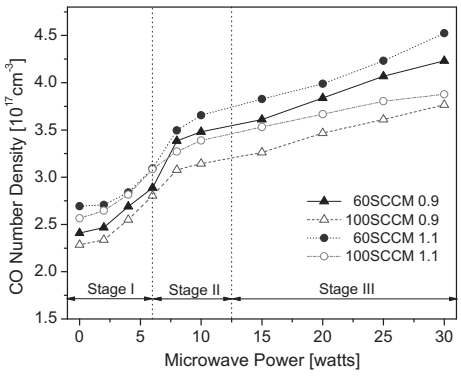

Fig. 7. CO number density in burnt gas of CH_4/O_2 flame vs. microwave powers at the same conditions as in Fig. 5 using CO Two-Photon Laser Induced Fluorescence.

Overall CO number density increases with microwave power for all conditions. In Stage 1, the in-situ fuel reforming (to hydrogen and carbon monoxide) as well as the temperature increase is expected to contribute to the enhancement in flammability limits and flame speed. It appears from Fig. 7 that the increase in CO is most dramatic near the intersection of stages 1 and 2, and tends to be linear towards the end of stage 2 and into stage 3. This is because the fraction of microwave power that goes into fuel reforming is larger near stages 1 and 2, whereas more power is directed towards ionization of gases in stages 2 and 3.

CO production in rich flames is generally higher than that in lean flames. This is confirmed in the first data point (0 W microwave power) of all four series. But in Stages 2 and 3 when microwave power is higher, CO number density at 100 SCCM with $\phi = 0.9$ is higher than that at 60 SCCM with $\phi = 1.1$. This is because at higher microwave power range, the effects of fuel breakdown from the plasma discharge surpass the thermal CO production in the flame. With lower flow rates, microwave energy distribution per particle will be larger. Therefore, at lower microwave powers (Stage 1), CO production is higher for rich conditions while at higher microwave powers (Stages 2 and 3), CO production for lower total flow rate is higher than that of higher flow rate. Also at higher flow rate, residence time (time that mixture gas reacts with discharge) is shorter than that at lower flow rate.

It is of great interest to quantify of the degree of fuel reforming assisted by the plasma. Syn-gas generation has other practical implications in terms of hydrogen generation [32,33]. CO number density increases to 3.88×10^{17} cm^{-3} at the highest microwave power of 30 W, from 2.57×10^{17} cm^{-3} without microwave at the same flow condition (100 SCCM and $\phi = 1.1$). Mole fraction was calculated using rotational temperature in previous section, and CO mole fraction increases approximately from 15% to 9% without microwave in the same condition. Assuming that the water is in vapor state, in our configuration, 18% of the total methane undergoes reforming to syn-gas at 30 W of microwave power, which is significant considering the competing oxidation reactions which subsequently leads to CO_2.

4. Conclusions

A newly designed microwave re-entrant cavity applicator discharge system is used for plasma enhanced combustion of methane/oxygen mixtures. Three distinct stages were observed, depending on input microwave power. In Stage 1 where

microwave energy is low and only the electric field couples to the flame, flammability and flame speed are increased, and slight increases in temperature due to ohmic heating and more in-situ fuel reform are observed. As microwave power increases, OH radicals and fuel reforming are increased and a plasma plume is initiated. As the microwave power is increased further, the reaction zone is overlapped by a full plasma plume; OH number density is relatively constant, but CO concentration increases further. In this stage, the plasma discharge can be sustained without combustion and can the ignite methane/oxygen mixture. The direct coupling of electromagnetic energy can be utilized for various levels of combustion enhancement and ignition for practical combustion systems including flame holding for harsh transient operating conditions. Further studies to indentify individual mechanisms during the flame enhancement are required.

Acknowledgments

This work was supported by the AFOSR (Award# FA9550-09-1-0282) with Dr. Julian Tishkoff as Technical Monitor and through the Michigan State University IRGP Funding.

References

[1] S.M. Starikovskaia, *Journal of Physics D: Applied Physics* 39 (2006) R265–R299.
[2] A.Y. Starikovskii, *Proceedings of the Combustion Institute* 30 (2005) 2405–2417.
[3] A.B. Leonov, D.A. Yarantsev, A.P. Napartovich, I.V. Kochetov, Plasma-assisted ignition and flame-holding in high-speed flow, in 44th AIAA Aerospace Sciences Meeting, AIAA-2006-563, 2006.
[4] S.B. Leonov, D.A. Yarantsev, *Plasma Sources Science and Technology* 16 (2007) 132–138.
[5] T. Ombrello, Y. Ju, A. Fridman, *AIAA J.* 46 (2008) 2424–2433.
[6] T. Ombrello, S.H. Won, Y. Ju, Lifted flame speed enhancement by plasma excitation of oxygen, in: 47th AIAA Aerospace Sciences Meeting and Exhibit, AIAA-2009-689, 2009.
[7] W. Kim, H. Do, M.G. Mungal, M.A. Cappelli, *IEEE Transactions on Plasma Science* 34 (2006) 2545–2551.
[8] W. Kim, M. Godfrey Mungal, M.A. Cappelli, *Combustion and Flame* 157 (2010) 374–383.
[9] E. Mintusov, A. Serdyuchenko, I. Choi, W.R. Lempert, I.V. Adamovich, Mechanism of plasma assisted oxidation and ignition of ethylene–air flows by a repetitively pulsed nanosecond discharge, in: 46th AIAA Aerospace Sciences Meeting and Exhibit, AIAA 2008-1106, 2008.
[10] M. Uddi, N. Jiang, E. Mintusov, I.V. Adamovich, W.R. Lempert, Atomic oxygen measurements in air and air/fuel nanosecond pulse discharges by two photon laser induced fluorescence, in: 46th AIAA Aerospace Sciences Meeting and Exhibit, AIAA 2008-1110, 2008.
[11] E.S. Stockman, S.H. Zaidi, R.B. Miles, C.D. Carter, M.D. Ryan, *Combustion and Flame* 156 (2009) 1453–1461.
[12] K.W. Hemawan, I.S. Wichman, T. Lee, T.A. Grotjohn, J. Asmussen, *Review of Scientific Instruments* 80 (2009) 053507.
[13] R.M. Fredericks, J. Asmussen, *Journal of Applied Physics* 42 (1971) 3647–3649.
[14] K. Kohse-Hoinghaus, J.B. Jeffries, *Applied Combustion Diagnostics*, Taylor & Francis, 2002.
[15] P.H. Paul, *J. Quant. Spectrasc. Radiat. Transfer* 51 (1994) 511–524.
[16] J.M. Seitzman, J. Haumann, R.K. Hanson, *Applied Optics* 26 (1987) 2892–2899.
[17] GRI-Mech 3.0 http://www.me.berkeley.edu/gri-mech/version30.
[18] T. Pedersen, R.C. Brown, *Combustion and Flame* 94 (1993) 433–448.
[19] Y. Ju, S.O. Macheret, M.N. Shneider, R.B. Miles, D.J. Sullivan, Numerical study of the effect of microwave discharge on the premixed methane–air flame, in: 40th AIAA/ASME/SAE/ASEE Joint Propulsion Conference and Exhibit, 2004.
[20] R. Ono, T. Oda, *IEEE Transaction on Industry Applications* 37 (2001) 709–714.
[21] W. Kim, H. Do, M.G. Mungal, M.A. Cappelli, *Proceedings of the Combustion Institute* 31 (2007) 3319–3326.
[22] G. Pilla, D. Galley, D.A. Lacoste, F. Lacas, D. Veynante, C.O. Laux, *IEEE Trans. on Plasma Science* 34 (2006) 2471–2477.
[23] K. Shinohara, N. Takada, K. Sasaki, *Journal of Physics. D. Applied Physics* 42 (2009) 182008, 182004pp.
[24] S.H. Zaidi, E. Stockman, X. Qin, Z. Zhao, S. Macheret, Y. Ju, R.B. Miles, D.J. Sullivan, J.F. Kline, Measurements of hydrocarbon flame speed enhancement in high-Q microwave cavity, in: 44th AIAA Aerospace Sciences Meeting and Exhibit, AIAA-2006-1217, 2006.
[25] M. Uddi, Non-equilibrium kinetic studies of repetitively pulsed nanosecond discharge plasma assisted combustion, in: Department of Mechanical Engineering, Ohio State University, 2008.
[26] P.W.J.M. Boumans, *Inductively Coupled Plasma Emission Spectroscopy*, John Wiley & Sons, New York, Chichester, Brisbane, Toronto, Singapore, 1987.
[27] J. Happold, P. Lindner, B. Roth, *Journal of Physics. D. Applied Physics* 39 (2006) 3615–3620.
[28] S. Pellerin, J.M. Cormier, F. Richard, K. Musiol, J. Chapelle, *Journal of Physics. D. Applied Physics* 29 (1996) 726.
[29] H.P. Broida, *Journal of Chemical Physics* 21 (1953) 1165–1169.
[30] A.G. Gaydon, H.G. Wolfhard, Flames, their structure, radiation and temperature, 273, 1970.
[31] E.S. Stockman, J.B. Michael, A. Fuller, S.H. Zaidi, R.B. Miles, Toward high Q evanescent coupled microwave controlled combustion, in: 47th AIAA Aerospace Sciences Meeting Including The New Horizons Forum and Aerospace Exposition, 2009.
[32] L. Bromberg, D.R. Cohn, A. Rabinovich, J. Heywood, *International Journal of Hydrogen Energy* 26 (2001) 1115–1121.
[33] L. Bromberg, D.R. Cohn, A. Rabinovich, N. Alexeev, *International Journal of Hydrogen Energy* 24 (1999) 1131–1137.